

Heat transfer in MHD square duct flow of nanofluid with discrete heat sources

Kozhikkatil Sunil Arjun*, Rakesh Kumar

Indian Institute of Technology (ISM) Dhanbad, India

Received 3 June 2017;

revised 3 March 2018;

accepted 25 May 2018;

available online 3 July 2018

ABSTRACT: The effect of thermal and solutal buoyancy induced by a discrete source of heat and mass transfer in a square duct under the influence of magnetic field, especially at the turbulent regime for the first time is reported. Al_2O_3 /water nanofluid is used with constant heat flux from three discrete heat sources. In the present study, the effects of Reynolds number (100 to 3000), particle volume fraction (0 to 2%) and magnetic field ($\text{Ha} = 10$ to 90) on the Nusselt number, pressure drop and wall temperature (at the axial and height directions) are represented graphically and discussed quantitatively. Two percent Al_2O_3 -water nanofluid under $\text{Ha} = 10$ can produce 81% increase in Nusselt number with only 60% increase in pressure drop when compared to base fluid at $\text{Re} = 100$. Four percent enhancement in nanofluids cooling effect in the vicinity of a centre of the final heat source can be utilized in hot spots cooling.

KEYWORDS: discrete heat source; heat transfer; Magneto Hydro Dynamics; Nusselt number; square duct

INTRODUCTION

The large air flow rate needs more powerful fans, thereby producing system noise and vibration, and Air-cooling is limited to chip level heat fluxes of only about 1 W/cm^2 [1]. Liquid cooling has been considered as more effective for removing heat than air-cooling and it may be the only practical method for maintaining reasonable component temperatures in the high power chips [2]. The relative performance and features of cooling modes for gas and liquid have been described [3]. Despite its attractive thermal attributes, direct liquid cooling with or without phase change has not gained widespread popularity in the mainframe computer industry, largely due to the lack of understanding of the heat transfer properties for dielectric coolant.

Hot spots have an adverse influence on performance and operation conditions of them due to ample produced energy which must be evacuated from the system. Passive heat transfer enhancement can be obtained by changing the geometry or modifying thermal properties of working fluid [4].

With the growing of power density of electronic components, considerable attention has recently turned to mixed convection in ducted flow from discrete heat sources because of a number of practical applications including electronic cooling systems, heat exchangers, and solar collectors.

The effort is required to maintain an acceptable operating temperature below an allowable level of about 85°C . Magnetohydrodynamic (MHD) flow in ducts in the presence of a transverse magnetic field occur in metallurgical processing applications, and within the cooling blankets enveloping magnetic confinement fusion reactors.

*Corresponding Author Email: arjun@mece.ism.ac.in
Tel.: +7587532033; Note. This manuscript was submitted on June 3, 2017; approved on May 25, 2018; published online July 3, 2018.

Other liquid-metal duct flow applications include the cooling of nuclear fission reactors and high-performance computing infrastructure.

Beyond MHD applications, channel flows exhibiting quasi-two-dimensional characteristics appear in applications ranging from microfluidics to geophysical flows. Cooling of combustion chambers of the rocket engines, heat exchangers, tunnels fires etc. are other applications of duct flow with hot spots. The thermal conductivity of Ag_2Al -water and Al_2Cu -water nanofluids have been reported to increase by about 130% with a volume fraction less than 1% [5].

The effect of CuO -water nanofluid as a cooling medium to simulate the heat transfer behavior in a two-dimensional (infinite depth) horizontal rectangular duct, where the top and bottom walls were two isothermal symmetric heat sources have been investigated numerically [6]. They reported that the heat transfer enhancement is possible using nanofluid in comparison with conventional fluid for Newtonian as well as non-Newtonian cases. Alumina-water nanofluid produces smoother flow fields and temperature distributions and heat transfer rate increases between parallel disks with higher volume fraction, smaller nanoparticle diameter, reduced disk-spacing and larger inlet Reynolds number [7]. The use of nanofluid can produce an asymmetric velocity along the height of the parallel plates channel with discrete heat sources and the wall temperature decreases remarkably as Re and ϕ increase [8]. Experimental study of Al_2O_3 /water nanofluid through the square cross-sectional duct under constant heat flux in laminar flow showed enhancement of heat transfer coefficient up to 27.6% at 2.5% volume fraction and the increments were more pronounced at high flow rates with a decrement of wall temperatures [9].

Nomenclature			
A	Area (m ²)	y	At y direction
Bc	Boltzmann constant	Greek Symbols	
Bo	Applied Magnetic field	α	Thermal diffusivity (m ² /s)
Cp	Specific heat of the fluid (J/kg K)	β	Thermal expansion coefficient (K ⁻¹)
CFD	Computational Fluid Dynamics	μ	Dynamic viscosity (kg/ms)
d	Size of particle or molecule (m)	ν	Kinematic viscosity (m ² /s)
E	Energy (J)	ρ	Density (kg/m ³)
F	Total body forces	σ	Electrical conductivity (Sm ⁻¹)
F	Friction factor	ϕ	Particle volume fraction (%)
g	Acceleration due to gravity (m/s ²)	Δp	Pressure drop (kPa)
h	Heat transfer coefficient through the heat sources (W/m ² K)	τ_{eff}	Effective stress tensor
H	Channel height (m)	∇	Nabla operator (1/m)
Ha	Hartmann number		Subscripts
k	Thermal conductivity (W/m K)	ave	Average
l	Mean free path (m)	bf	Base fluid
Nu	Local Nusselt number	m	Mean
p	Pressure (kPa)	nf	Nanofluid
q''	Heat flux of heat sources (W/m ²)	p	Particles
Re	Reynolds number	s	Surface
T	Temperature (K)	w	Wall
VV	Velocity vector (m/s)	0	Inlet conditions

By increasing the Reynolds number, volumetric concentration and decreasing the size of nanoparticles, Nusselt number and heat transfer coefficient have been enhanced assuming that there is constant heat flux boundary condition at walls and using dispersion model and solving the system numerically [10]. By adding nanoparticles, increase of faces of non-circular ducts and by use of CuO/water nanofluid instead of Al₂O₃/water nanofluid, pressure drop increases in the laminar flow of square and triangular cross-sectional ducts. CFD predictions of laminar mixed convection of Al₂O₃/water nanofluid by single-phase and three different two-phase models (volume of fluid, mixture and Eulerian) have been studied [11]. Mixed convection in the inclined square lid-driven cavity filled with Al₂O₃/water nanofluid [12] and nanofluid flow over periodic rib-grooved channels in turbulent flow was studied [13]. Comparison of Nusselt numbers resulted from the simulation and experimental results for 20 nm Al₂O₃/water nanofluid [10] versus Peclet number in triangular duct [14] were within the limits with a maximum discrepancy of 9%.

Laminar flow using 8% CuO/water nanofluid through an equilateral triangular duct at constant wall heat flux resulted in heat transfer increases up to 41% [15]. By offsetting a circular cylinder from the wake centreline, 48% heat transfer enhancement from the side-wall of a rectangular duct through which an electrically conducting fluid flows within a strong transverse magnetic field is achieved with only a modest increase in pressure drop [16]. The bulk instability is more typical to MHD mixed-convection rectangular duct flows with volumetric heating at relatively low Reynolds and high Grashof numbers such that the basic

velocity profile demonstrates a high-velocity jet near the hot wall and two or more inflection points, which influence turbulent transition [17]. For mixed convection, there is no correlation reported except for predicting the average Nusselt number for the case of discrete flush-mounted heat source [18]. The location of the heater element does not play a considerable role in the heat transfer processes. For low Reynolds number, heat transfer is mainly controlled by Grashof number and cooling is more effective compared to forced and natural convection [19].

For the flush-mounted and protruded discrete heat source, natural convection plays an important role in the total heat transfer process, leading to a possible mixed convection behavior. The protruding heat source distorts the flow field significantly and causes the transition from laminar to turbulent flow at a lower Reynolds number, and enhances the forced convection significantly [20]. As the Reynolds number increases, the heat transfer by protruding chips is always greater than that by flush chips [21]. In the mixed regime, the location of the heater is less important, and at low Reynolds number, heat transfer is mainly controlled by the Grashof number [22].

Two different analytical approaches are utilized [23] to determine how to arrange discrete heat sources on wall cooled by forced convection: a large number of small heat sources and a small number of heat sources with a finite length, which are placed on a flat wall. Both analyses showed that heat sources should be mounted non-uniformly on the wall to obtain better heat transfer rate. The fluid flow and heat transfer characteristics associated with cooling an inline array of discrete heated blocks in a channel by using a single laminar slot air jet have been examined [24]. The

heat transfer rate increases with the increase of Reynolds number and the decrease of channel height and the effective cooling of blocks increase for shorter and widely spaced heated blocks.

The discrete heat sources should be distributed non-uniformly on a wall of a convergent flow [25] and the optimal spacing between heat sources depends on both Reynolds number and channel shape factor. The wall temperature is higher for lower Reynolds number due to the higher residence time of fluid particles [26].

The above literature shows that the effect of thermal and solutal buoyancy has not been widely studied and no computational studies have been found for the effect of the buoyancy induced by a discrete source of heat and mass transfer in a square duct under the influence of magnetic field.

The purpose of this paper is to report on a computational study of developing mixed convection heat and mass transfer in a square duct using nanofluid, at laminar and turbulent regimes with hot spots and weak magnetic field. Discrete heat sources with a uniform heat flux are mounted on the bottom wall and rest of the wall is considered. Applied nanofluid is composed of distilled water and Al₂O₃ nanoparticles. The flow and heat transfer characteristics and thermo-physical properties are evaluated and discussed quantitatively.

GEOMETRY, GOVERNING EQUATIONS AND SIMULATION

In the present study of heat transfer to turbulent nanofluid in a square duct, the standard k-ε turbulent model was used. Considered the nanofluid as a continuous media with thermal equilibrium and flow at same velocity. The nanofluid is incompressible with temperature-dependent properties.

The compression work and viscous dissipation terms are negligible.

Effects of the Al₂O₃-water nanofluid having 25 nm mean diameter nanoparticles on heat transfer rate and pressure drop of flow with hot spots are studied in this paper. A transverse magnetic field with variable strength B₀ is applied parallel to the y- axis.

There is no applied voltage and the magnetic Reynolds number is small, hence the induced magnetic field and Hall effects are negligible.

The phenomenon under consideration is governed by the steady two-dimensional form of the continuity, the Navier-Stokes equation and energy equation.

$$\nabla(\rho_{nf}V) = 0 \quad (1)$$

$$\nabla \cdot (\rho_{nf}VV) = -\nabla P + \mu_{nf}\nabla^2V + F_y \quad (2)$$

$$F_y = -\frac{Ha^2\mu_{nf}}{H^2}v + (\rho\beta)_{nf}g_y(T - T_m) \quad (3)$$

Where

$$Ha = -HB_0\sqrt{\frac{\sigma_{nf}}{\mu_{nf}}} \quad (4)$$

ANSYS FLUENT solves the energy equation in the following form:

$$\frac{\partial}{\partial t}(\rho E) + \nabla \cdot (\vec{v}(\rho E + p)) = \nabla \cdot (k_{eff}\nabla T - \sum_j h_j\vec{J}_j + (\bar{\tau}_{eff} \cdot \vec{v})) + S_h \quad (5)$$

Where k_{eff} is the effective conductivity ($k + k_t + k_b$, where k_t is the turbulent thermal conductivity and k_b is the thermal conductivity due to Brownian motion of nanoparticles in the duct), and \vec{J}_j is the diffusion flux of species J . The first three terms on the right-hand side of Equation represent energy transfer due to conduction, species diffusion, and viscous dissipation. S_h includes the heat of chemical reaction, and any other volumetric heat sources.

$$E = h - \frac{p}{\rho} + \frac{v^2}{2} \quad (6)$$

Where sensible enthalpy h is defined as

$$h = \sum_j Y_j h_j \quad (7)$$

Y_j is the mass fraction of species j .

$$h_j = \int_{T_{ref}}^T c_{p,j}dT \quad (8)$$

T_{ref} is used as 300 K.

The equations 1, 2 and 5 are solved by using proper boundary conditions.

The boundary conditions of a uniform velocity at the inlet equal to V_0 , no-slip at the walls, zero relative pressure at the outlet, a uniform temperature at entrance equal to T_0 , adiabatic condition at walls, except along heat sources, where a uniform heat flux equal to 20 kW/m² is applied. A uniform mass flow rate was assigned at the channel inlet. Discrete heat sources with a uniform heat flux are mounted on the bottom wall and rest of the wall are considered adiabatic.

Density, Specific heat and Viscosity are defined as follows:

$$\rho_{nf} = (1 - \varphi)\rho_{bf} + \varphi\rho_p \quad (9)$$

$$(C_p)_{nf} = (1 - \varphi)(C_p)_{bf} + \varphi(C_p)_p \quad (10)$$

and

$$\mu_{nf} = \mu_{bf} \exp[4.91\varphi(0.2092 - \varphi)] \quad (11)$$

Where

$$\mu_{bf} = 0.02165 - 0.0001208T + 1.7184 \times 10^{-7}T^2 \quad (12)$$

The turbulence kinetic energy, k , and its rate of dissipation, ε , are obtained solving the following transport equations:

$$\frac{\partial}{\partial t}(\rho k) + \frac{\partial}{\partial x_i}(\rho k v_i) = \frac{\partial}{\partial x_j} \left[\left(\mu + \frac{\mu_t}{\sigma_k} \right) \frac{\partial k}{\partial x_j} \right] + G_k + G_b - \rho \varepsilon - Y_M + S_k \quad (13)$$

and

$$\frac{\partial}{\partial t}(\rho \varepsilon) + \frac{\partial}{\partial x_i}(\rho \varepsilon v_i) = \frac{\partial}{\partial x_j} \left[\left(\mu + \frac{\mu_t}{\sigma_\varepsilon} \right) \frac{\partial \varepsilon}{\partial x_j} \right] + C_{1\varepsilon} \frac{\varepsilon}{k} (G_k + C_{3\varepsilon} G_b) - C_{2\varepsilon} \rho \frac{\varepsilon^2}{k} + S_\varepsilon \quad (14)$$

In these equations, G_k represents the generation of turbulence kinetic energy due to the mean velocity gradients. G_b is the generation of turbulence kinetic energy due to buoyancy.

Y_M represents the contribution of the fluctuating dilatation in compressible turbulence to the overall dissipation rate. $C_{1\varepsilon}$, $C_{2\varepsilon}$ and $C_{3\varepsilon}$ are constants. σ_k and σ_ε are the turbulent Prandtl numbers for k and ε respectively. S_k and S_ε are user-defined source terms.

The turbulent viscosity μ_t is computed by combining k and ε as follows:

$$\mu_t = \rho C_\mu \cdot \frac{k^2}{\varepsilon} \quad (15)$$

The model constant $C_{1\varepsilon}$, $C_{2\varepsilon}$, $C_{3\varepsilon}$, C_μ , σ_k and σ_ε have the default values of 1.44, 1.92, 1, 0.09, 1 and 1.3 respectively. Brownian motion and mean diameter of nanoparticles are considered for defining thermal conductivity.

$$\frac{k_{nf}}{k_{bf}} = 1 + 64.7\varphi^{0.7466} \left(\frac{d_{bf}}{d_p} \right)^{0.3690} \left(\frac{k_p}{k_{bf}} \right)^{0.7476} \times \left(\frac{2.4 \times 10^{-5} \times 10^{247-140}}{\rho_{bf} \alpha_{bf}} \right)^{0.9955} \times \left(\frac{\rho_{bf} B_c T}{3\pi \left(2.4 \times 10^{-5} \times 10^{247-140} \right)^2 l^2 b_{bf}} \right)^{1.2321} \quad (16)$$

The thermal performance of the duct is characterized in terms of average heat transfer coefficient through the heat sources.

$$h_{ave} = \frac{\int h_s dA}{3H^2} \quad (17)$$

where

$$h_s = \frac{q''}{(T_m - T_0)} \quad (18)$$

Thermal performance of the duct is characterized in terms of Nusselt number. Nu is calculated using the following equation.

$$Nu = \frac{q'' H}{k (T_w - T_m)} \quad (19)$$

The pressure drop is determined as:

$$\Delta p = f \rho v^2 / 2H^2 \quad (20)$$

The governing differential equations are solved using the finite volume method. A second order upwind method is used for energy and momentum equations. The SIMPLE procedure is chosen to couple pressure and velocity. Axis symmetry was assigned at centerline. The solution convergence is met when the normalized residuals reach to the 10^{-6} for all equations with the help of Ansys Fluent 15.0. The default values of under relaxation factor used in the simulation work are 0.3 for pressure, 0.7 for momentum and 1 for density, body force and energy.

A two-dimensional geometry of nanofluid laminar and turbulent forced convection in square duct under the influence of magnetic field is presented in Figure 1. Three heat sources of length H (one-tenth of a side of duct cross section) are placed on the bottom wall of the channel. The spacing between heat sources is also equal to H and the side of the duct is 100 mm.

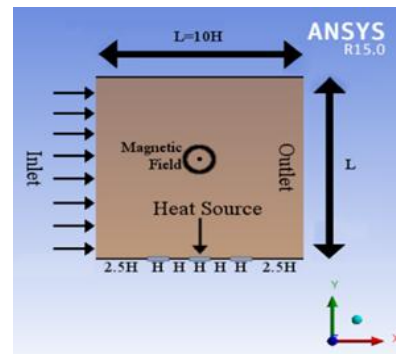


Fig. 1. Geometry of square duct with discrete heat sources

VALIDATION

The effect of grid size on the predicted temperature at the middle of the last heat source in height direction for $Re = 100$ and $\phi = 2\%$. As it can be seen a grid density of 17×250 provides an acceptable solution for the laminar regime. The grid used in the present analysis is non-uniform with highly packed grid points in the vicinity of the duct wall and especially in the entrance region. The calculations were also performed for the same volumetric concentration at $Re = 1980$ and the computational mesh consisting of 50×250 grid points was found possible for the fully-developed turbulence regime. Table 1 shows the results of the grid sensitivity analysis.

Table 1
Result of grid independence test.

Laminar Regime		Turbulent Regime	
Number of grids	Temperature (K)	Number of grids	Temperature (K)
17x200	318.723	50x200	353.029
17x250	318.614	50x250	352.927
17x300	318.611	50x300	352.929

Validation of simulated data with the published data of [27] using Al_2O_3/H_2O nanofluid in square duct resulted in only a 0.8% deviation in Nu value at 5% volume concentration at $Re = 1347$, which verifies the accuracy and reliability of the numerical code. The model [9] was validated with the experimental data of [28], which was further validated in that manuscript [27].

RESULTS AND DISCUSSION

Temperature field

Since the variations of temperature on the top wall are negligible, the same is illustrated only for bottom wall. Figure 2 shows the cooling benefits of Al_2O_3 -water nanofluid on discrete heat source affected bottom wall of the square duct by the wall temperature as a function of channel length for various volume fractions for $Re = 100$.

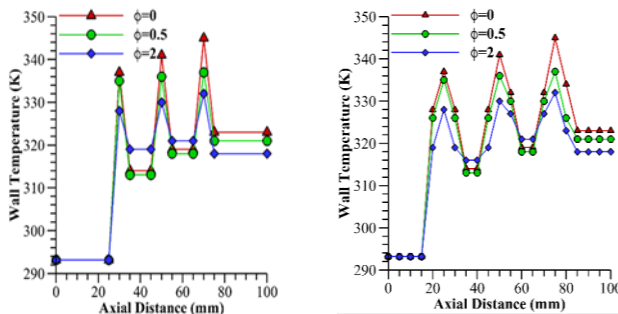


Fig. 2. Effect of ϕ on bottom wall temperature along channel length at $Re = 100$

It can be seen that wall temperature decreases as nanoparticle volume fraction increases for all considered cases up to 2% and the same lower magnitude effect exist

for axial variation of temperature upon increase of nanoparticle volume fraction. The wall temperatures were higher to the last of each heat source, while lower to those belonging to the end of each adiabatic section. The greatest values of wall temperature are related to the end of last heat source, while the smallest to the end of last adiabatic section.

The distance up to 15 mm is the thermally developing region of the flow in the square duct and depicts the entrance temperature, without any natural convection effect, as the first heat source is positioned at 25 mm away from the entrance and the rest of the walls other than the heat sources are kept adiabatic. The values of temperature at the middle of the last heat sources in height direction for $Re = 100$ are depicted in Figure 3 for different volume fractions.

As illustrated in this figure, adding nanoparticle into base fluid decreases temperature up to 4% especially near the heat sources and the greatest decrease recorded at 40% height from the bottom wall. The variation in temperature could be noticed up to 20% height and the optimal height lies in between 20% and 40%.

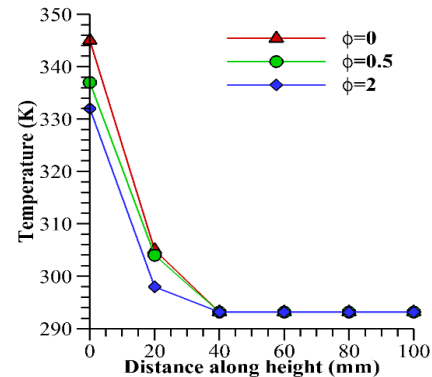


Fig. 3. Effect of ϕ on temperature at center of last heat source along the height at $Re = 100$

Heat transfer

Results show that the existence of nanoparticles has a significant effect on heat transfer enhancement, without the influence of magnetic field.

The Nusselt number and pressure drop profiles as a function of Reynolds number and nanoparticle volume fraction are depicted in Figure 4 without the influence of magnetic field.

The Nusselt number increases up to 225% as Reynolds number is increased.

It is also observed that as ϕ increases Nu becomes higher for a fixed value of Re and greatest increase up to 41% was observed for $Re = 100$.

Thus, passing from $\phi = 0\%$ to $\phi = 2\%$, the greatest value of about 14.1 for Nu is found at $Re = 3000$ and $\phi = 2\%$.

The changes in the trend of variation after Re 1980 in Figure 4 might be due to the stabilization of turbulent regime at that Re.

Figure 5 illustrates the Nusselt number, referred to the magnetic field strength values calculated, as a function of Reynolds number for $\phi = 2\%$.

There is a much augmentation for the Nusselt number at all Re in comparison without the influence of magnetic field at Ha = 10, with the highest improvement of 29% for Re = 100. As Re increases, though Nu increases, the influence of magnetic field decreases drastically to 4% at Re = 3000. All higher magnetic field strengths recorded lower Nusselt numbers than using water without magnetic field influence and as Ha increases, Nusselt number decreases.

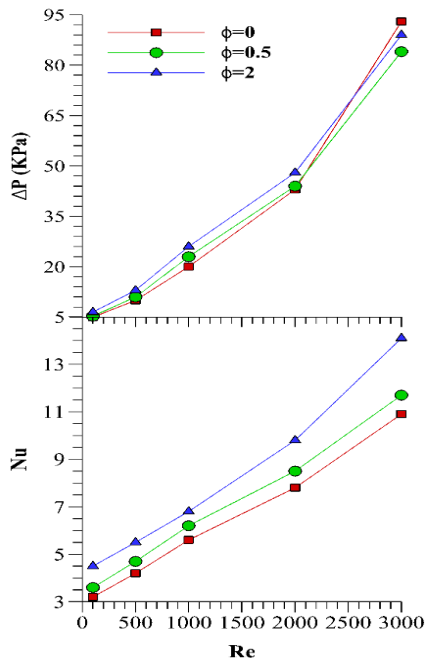


Fig. 4. Effect of ϕ and Re with Ha = 0 on Nu and pressure drop

Pressure drop

The use of nanoparticles in base fluid can have an unpleasant influence on pressure drop because of increased viscosity. The pressure drop profiles as a function of Reynolds number are illustrated in Figure 4 for $\phi = 0, 0.5$ and 2% and it increased up to 19 fold from Re 100 to 3000. The pressure drop increases as Reynolds number and particle volume fraction increase and the greatest value about 89 Pa are detected at Re = 3000 and $\phi = 2\%$. The pressure drop increased up to 30% as particle volume fraction increased from 0 to 2%, with the increase more clear at lower Re with a drastic decrease to 12% at transition regime.

The pressure drop showed a decreasing trend at Re = 3000 up to 5% when the volume fraction increased from 0 to 2%.

The pressure drop, subjected to the magnetic field is described in Figure 5. It is observed that Δp is greater than that without the magnetic field for all considered cases at Ha = 10 and at 2% nanoparticle volume concentration up to 23% with a reduction in the ratio of improvement as Re increases up to transition regime, but showed a further hike at the turbulent regime. Even then, the pressure drop values increased drastically as Re increases at all magnetic field strengths.

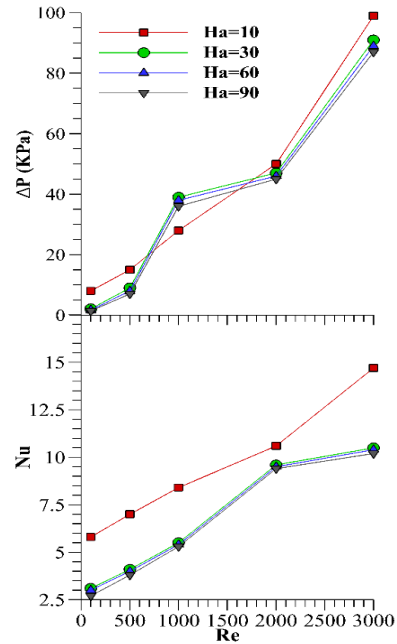


Fig. 5. Effect of Ha and Re with $\phi = 2\%$ on Nu and pressure drop

As Ha increases, pressure drop decreases up to 6 fold with a decreasing trend as Re increases up to transition regime and at turbulent zone registered a comparative increase from the previous Re. Analogous to Nu, there is drastic change of pressure drop with performance index lower than one for most of the Re and Ha. It is found that the performance index, the index of better thermal behavior of nanofluid, is greater than one for Re = 100 when subjected to magnetic field strength of Ha from 30 to 90 with the greatest value of 1.93 at Ha = 90.

CONCLUSIONS

A two-dimensional numerical analysis of flow and heat transfer characteristics of nanofluid in a square duct with discrete heat sources has been carried out. A novel simulation model for the effect of thermal solutal buoyancy is developed afresh using Fluent 15.0. The new model takes several mechanisms into proper consideration, including Brownian motion, mean diameter of nanoparticles and mixed convection flow. Adding nanoparticle into base fluid decreases temperature up to 4% near the heat sources. Nu registered maximum increase of 41% at lower Re. There is

29% augmentation for Nu with the influence of weaker magnetic field at $Ha = 10$ for lower Re. The pressure drop increased up to 30% as particle volume fraction increased to 2%, with the increase more clear at lower Re with a drastic decrease to 12% at transition regime and a further 5% decreasing trend at the turbulent zone. The performance index is greater than one for lower Re when subjected to magnetic field strength of Ha from 30 to 90 with the greatest value of 1.93 at $Ha = 90$. Results clearly show that the use of nanofluid with temperature-dependent properties can significantly increase heat transfer rate near the heat sources, where higher heat evacuation is required such as hot spots. The new numerical model can be used to predict the temperature decline and optimize the discrete heat source limits of the electronic cooling.

REFERENCES

- [1] Nakayama W, Bergles AE. Cooling Electronic Equipment; Past, Present, and Future. *Heat Transfer in Electronic and Microelectronic Equipment*. 1990:3-9.
- [2] Mudawar I. Direct-immersion cooling for high power electronic chips. In *Thermal Phenomena in Electronic Systems*, 1992. I-THERM III, InterSociety Conference on 1992 Feb 5 (pp. 74-84). IEEE.
- [3] Bar-Cohen A. Physical design of electronic systems—methodology, technology trends, and future challenges. *Advances in Thermal Modeling of Electronic Components and Systems*. 1993;3:1-60.
- [4] Sasmito AP, Kurnia JC, Mujumdar AS. Numerical evaluation of laminar heat transfer enhancement in nanofluid flow in coiled square tubes. *Nanoscale research letters*. 2011 Dec 1;6(1):376.
- [5] Chopkar M, Sudarshan S, Das PK, Manna I. Effect of particle size on thermal conductivity of nanofluid. *Metallurgical and Materials Transactions A*. 2008 Jul 1;39(7):1535-42.
- [6] Santra AK, Sen S, Chakraborty N. Study of heat transfer due to laminar flow of copper–water nanofluid through two isothermally heated parallel plates. *International Journal of Thermal Sciences*. 2009 Feb 1;48(2):391-400.
- [7] Feng Y, Kleinstreuer C. Nanofluid convective heat transfer in a parallel-disk system. *International Journal of Heat and Mass Transfer*. 2010 Oct 1;53(21-22):4619-28.
- [8] Mashaei PR, Hosseinalipour SM, Bahiraei M. Numerical investigation of nanofluid forced convection in channels with discrete heat sources. *Journal of Applied Mathematics*. 2012;2012.
- [9] Heris SZ, Nassan TH, Noie SH, Sardarabadi H, Sardarabadi M. Laminar convective heat transfer of Al_2O_3 /water nanofluid through square cross-sectional duct. *International Journal of Heat and Fluid Flow*. 2013 Dec 1;44:375-82.
- [10] Zeinali HS, Oghazian F, Khademi M, Saeedi E. Simulation of convective heat transfer and pressure drop in laminar flow of Al_2O_3 /water and CuO/water nanofluids through square and triangular cross-sectional ducts. *Journal of Renewable Energy and Environment*. 2015 Jan 1;2(1):7-19.
- [11] Akbari M, Galanis N, Behzadmehr A. Comparative analysis of single and two-phase models for CFD studies of nanofluid heat transfer. *International Journal of Thermal Sciences*. 2011 Aug 1;50(8):1343-54.
- [12] Fereidoon A, Saedodin S, Hemmat Esfe M, Noroozi MJ. Evaluation of mixed convection in inclined square lid-driven cavity filled with Al_2O_3 /water nano-fluid. *Engineering Applications of Computational Fluid Mechanics*. 2013 Jan 1;7(1):55-65.
- [13] Vatani A, Mohammed HA. Turbulent nanofluid flow over periodic rib-grooved channels. *Engineering Applications of Computational Fluid Mechanics*. 2013 Jan 1;7(3):369-81.
- [14] Heris SZ, Edalati Z, Noie SH, Mahian O. Experimental investigation of Al_2O_3 /water nanofluid through equilateral triangular duct with constant wall heat flux in laminar flow. *Heat Transfer Engineering*. 2014 Sep 2;35(13):1173-82.
- [15] Edalati Z, Zeinali Heris S, Noie SH. The study of laminar convective heat transfer of CuO/water nanofluid through an equilateral triangular duct at constant wall heat flux. *Heat Transfer—Asian Research*. 2012 Jul 1;41(5):418-29.
- [16] Hussam WK, Sheard GJ. Heat transfer in a high Hartmann number MHD duct flow with a circular cylinder placed near the heated side-wall. *International Journal of Heat and Mass Transfer*. 2013 Dec 1;67:944-54.
- [17] Smolentsev S, Vetcha N, Moreau R. Study of instabilities and transitions for a family of quasi-two-dimensional magnetohydrodynamic flows based on a parametrical model. *Physics of Fluids*. 2012 Feb;24(2):024101.
- [18] Bhowmik H, Tso CP, Tou KW, Tan FL. Convection heat transfer from discrete heat sources in a liquid cooled rectangular channel. *Applied Thermal Engineering*. 2005 Nov 1;25(16):2532-42.
- [19] Türkoğlu H, Yücel N. Mixed convection in vertical channels with a discrete heat source. *Mischkonvektion in vertikalen Kanälen mit einer lokalen Wärmequelle*. *Heat and Mass Transfer*. 1995 Feb 1;30(3):159-66.
- [20] Wang Y. Heat transfer and pressure loss characterization in a channel with discrete flush-mounted and protruding heat sources. *Experimental heat transfer*. 1999 Jan 1;12(1):1-6.

- [21] Tou KW, Xu GP, Tso CP. Direct liquid cooling of electronic chips by single-phase forced convection of FC-72. *Experimental Heat Transfer*. 1998 Apr 1;11(2):121-34.
- [22] Bhowmik H. Review on convection heat transfer in channel flow with discrete heater arrays for electronic cooling. *International Journal of Engineering, Science and Technology*. 2014;6(2).
- [23] Da Silva AK, Lorente S, Bejan A. Optimal distribution of discrete heat sources on a plate with laminar forced convection. *International Journal of Heat and Mass Transfer*. 2004 May 1;47(10-11):2139-48.
- [24] Arquis E, Rady MA, Nada SA. A numerical investigation and parametric study of cooling an array of multiple protruding heat sources by a laminar slot air jet. *International journal of heat and fluid flow*. 2007 Aug 1;28(4):787-805.
- [25] Jassim E, Muzychka YS. Optimal distribution of heat sources in convergent channels cooled by laminar forced convection. *Journal of Heat Transfer*. 2010 Jan 1;132(1):0117011-0117018.
- [26] Mashaei PR, Hosseinalipour SM, Bahiraei M, Dirani M. 3-D numerical simulation of nanofluid laminar forced convection in a channel with localized heating. *Australian Journal of Basic and Applied Science*. 2012;6:479-89.
- [27] Zeinali Heris S, Kazemi-Beydokhti A, Noie SH, Rezvan S. Numerical study on convective heat transfer of Al₂O₃/water, CuO/water and Cu/water nanofluids through square cross-section duct in laminar flow. *Engineering Applications of Computational Fluid Mechanics*. 2012 Jan 1;6(1):1-4.
- [28] Lyczkowski RW, Solbrig CW, Gidaspow D. Forced convection heat transfer in rectangular ducts—general case of wall resistances and peripheral conduction for ventilation cooling of nuclear waste repositories. *Nuclear Engineering and Design*. 1982 Feb 1;67(3):357-78.